Electric Power Systems Research 202 (2022) 107623

Contents lists available at ScienceDirect

Electric Power Systems Research

journal homepage: www.elsevier.com/locate/epsr

Wind farms in weak grids stability enhancement: SynCon or STATCOM?

Li Bao, Lingling Fan *, Zhixin Miao

Department of Electrical Engineering, University of South Florida, Tampa FL 33620, USA

ARTICLE INFO

Keywords:
Reactive power compensation
Synchronous condenser
STATCOM
Wind farm

ABSTRACT

Reactive power compensation is an effective method to enhance stability of a power system. Synchronous condenser (SynCon) and static synchronous compensator (STATCOM) are widely used for reactive power compensation. They have the capability of increasing system stability and efficiency by absorbing or generating reactive power. This paper presents a comparison of SynCon and STATCOM under the condition of zero reactive power injection. The two devices are integrated into a grid-connected type-4 wind farm to examine their effects on system stability. It is found that SynCon is more capable in stability enhancement compared to STATCOM. To explain the difference, we measure the *dq*-frame admittance frequency-domain responses of the two devices using frequency scans. Vector fitting method is then utilized to convert the admittance frequency-domain measurements to an *s*-domain model. The *s*-domain admittance-based eigenvalue analysis further confirms that SynCon is advantageous in stability enhancement. The difference of SynCon and STATCOM can be summarized as SynCon providing a steady-state reactance while STATCOM acting as a current source at steady state.

1. Introduction

Increasing penetrations of renewable energy sources such as wind farms have caused unexpected dynamic issues worldwide. In real-world operation, subsynchronous oscillations have been observed in the past decade in Texas, California, and China [1]. One type of oscillations is classified as weak grid oscillations by the IEEE PES Wind SSO task force report [1]. The low short circuit ratio (SCR) at the interconnection point is a factor that contributes to the oscillations. The mechanism of instability is similar as the traditional voltage stability: When wind power exporting level increases, the interconnection point voltage may decrease, as analyzed in [2,3]. The decrease in the ac voltage can cause a decrease in the exporting power; thus, an instability feedback mechanism is formed. Low SCR or weak grid interconnection makes this mechanism dominant and thus the system goes unstable [2,3].

In order to enhance voltage stability, reactive power compensation is an effective method. SynCon and STATCOM are two major devices for reactive power compensation. The objective of this paper is to compare the two devices in weak grid oscillation stability enhancement.

1.1. SynCon and STATCOM

SynCon have been applied in power systems with a long history. A reference in 1911 [4] presents the common applications of SynCon at that time. Essentially, a SynCon is a synchronous machine without a prime mover, working at motor operation. It is controlled by the excitation system to absorb or generate reactive power based on the requirement of power system. By the end of 2018, 90% of total generation capacity in Texas Panhandle area is wind generation. In order to enhance the stability and transmission efficiency, in April 2018, Electric Reliability Council of Texas (ERCOT) installed two SynCons with rated capacity of +175/-125 MVA at the 345 kV substations in Panhandle, resulting in 13% increase of power transfer compared to that in Year 2017 [5]. Reference [6] describes the project of installing four SynCons at 13.8 kV at Vermont Electric Power Company (VELCO)'s Granite 230/115 kV station in Williamstown Vermont. This upgrade project improved the reliability and stability of the Vermont power grid.

In recent decades, STATCOMs also have been widely utilized with the development of switching devices such as IGBT and GTO [7]. A STATCOM consists of a voltage source converter and a capacitor, which is capable of regulating reactive power transfer to the power system and the local voltage. Compared to a SynCon, STATCOM does not involve a rotating machine. It becomes the major reactive power device in the market. For example, in May 2001, the VELCO commissioned a project involving a STATCOM-based compensation system, which has a rated capacity of +133/-41 MVA, at Essex 115-kV station [8].

Even though both SynCons and STATCOMs are vastly installed by utility companies, SynCon has been used more in islanded power grids,

* Corresponding author.
E-mail address: linglingfan@usf.edu (L. Fan).

https://doi.org/10.1016/j.epsr.2021.107623
Received 9 April 2021; Received in revised form 3 September 2021; Accepted 3 October 2021
Available online 19 October 2021

e.g., Kauai of Hawaii, as shown in [9], and in zones with low SCR, e.g., South Australia [10]. Apart from reactive power compensation, SynCon is used to enhance grid strength and provide inertia and fault currents.

In this paper, we show that SynCon is more advantageous for weak grid stability enhancement.

1.2. Study approaches

Both electromagnetic transient (EMT) simulation and eigenvalue analysis are employed in this research to examine SynCon and STATCOM's performance for a type-4 wind farm with weak grid interconnection.

For eigenvalue analysis, we adopt *s*-domain admittance-based eigenvalue analysis. This method was proposed by Semleyn in 1999 [11] and has been found applications for inverter-based resource stability analysis recently [12]. The benefit of this approach is that we no longer need to derive a state-space model. Rather, we can obtain admittance model through measurements. This feature is especially useful for EMT simulation models. For example, the STATCOM model employed in this study is a 48-pulse GTO-based model. State-space modeling approach requires derivation of an average model in a dq-frame. On the other hand, this step is saved by utilizing measurements.

By applying a voltage harmonic disturbance at the device's terminal with a range of frequency and measuring the excited current response at the desired frequency, the frequency-domain measurement of an admittance can be obtained. To obtain an *s*-domain model or a transfer function from the frequency-domain response data, frequency-domain data fitting is required. Several packages of frequency-domain data fitting are available for use, e.g., the vector fitting package [13].

The objective of the vector fitting method is to fit a transfer function (matrix) to the frequency-domain measurements. The transfer function's order should be specified and the *s*-domain expression will be found. This can be done by minimizing the error between the measurement data and the frequency-response of the transfer function through iteratively tuning the parameters of the transfer function, e.g., poles and residues. In the end, a transfer function in *s*-domain can be found.

The vector fitting package in MATLAB is available in the public domain. In addition, MATLAB's system identification toolbox also offers tools, e.g., `tfest`, to estimate a transfer function from the frequency-domain response data [14].

With the *s*-domain admittances, eigenvalue analysis can be carried out for stability analysis.

1.3. Our contributions

There exists a large amount of literatures on comparison of SynCon and STATCOM. Reference [15] reviews the state-of-the-art reactive power compensation and their applications. The principles of operation and structures are also presented. Reference [16] demonstrates that SynCon and STATCOM have the similar dynamic performance at an HVDC system when subjected to a fault. Reference [17] proposes an inertial control for STATCOM, which provides better frequency response over SynCon.

In order to investigate the stability performance of STATCOM, [18] establishes the *dq*-domain small-signal impedance model of STATCOM by considering the phase-locked-loop (PLL) and other control loops, while reference [19] proposes the impedance model by injecting *dq*-domain perturbations. The two references determine the stability criterion through the Nyquist plots.

The aforementioned literatures treat SynCon and STATCOM as reactive power compensation devices, which enhance stability by regulating reactive power to the system. This paper investigates whether a SynCon or a STATCOM can improve the system stability for zero reactive power injection. We found that SynCon can improve stability while STATCOM has limited impact on the system under such condition.

In our preliminary work [20], we present EMT study results. In this paper, we present an explanation by comparing the *dq*-frame admittance measurements of the two devices. The frequency-domain measurements are obtained through harmonic injection or frequency scans. From the frequency-domain measurement data, the *s*-domain admittance model is obtained by vector fitting method [13]. Eigenvalue analysis based on *s*-domain admittance confirms the EMT simulation results.

1.4. Structure of this paper

This paper is organized as follows. Section 2 presents the EMT simulation results of a type-4 wind farm in a weak grid. The marginal stability condition is found through the EMT simulation. Furthermore, a SynCon or a STATCOM is integrated into the system to examine its effect. Section 3 presents the *dq*-admittance frequency-domain measurements of the wind farm, the STATCOM, and the SynCon using the harmonic injection method. The *s*-domain models are also approximated by vector fitting of the measurements. The admittance-based eigenvalue analysis results corroborate the EMT simulation results. This section also explains why there is a significant difference in stability enhancement through a comparison of the STATCOM and SynCon admittance models. Section 4 concludes this paper.

2. EMT simulation results

This section will introduce the EMT testbeds and the simulation result comparison for STATCOM and SynCon in a wind farm .

2.1. Wind farm

The investigated system is a type-4 wind farm connected to a grid through a transmission line. Fig. 1 presents the structure of the system. The terminal voltage of wind turbines is 575 V. The wind farm is connected to the 220-kV transmission system via two step-up transformers. The reactive power devices are connected to the grid through a 22-kV/220-kV transformer. The grid transmission network is comprised of two parallel lines. A circuit breaker is shown and switching on/off of the breaker changes the total transmission network impedance.

The type-4 wind farm is constituted by a synchronous machine, a machine-side converter (MSC) and a grid-side converter (GSC), which is connected to PCC through a choke filter. The GSC consists of an inner current control loop and outer voltage control loops, as shown in Fig. 2. The inner current controller generates the *dq*-frame voltage references, which will be further converted into the three-phase voltage references relying on a synchronized phase angle provided by a phase-locked-loop (PLL). The outer controllers are PCC voltage and DC-link voltage control. Since the PLL's d-axis is aligned with the PCC voltage's space vector, the *d*-axis PCC voltage v_d has the same magnitude as V_{PCC} and v_q keeps as zero at steady state. In the *dq*-frame, the expressions of active power and reactive power delivered from the GSC to the grid are:

$$\begin{aligned} P &= v_d i_d \\ Q &= -v_d i_q \end{aligned} \tag{1}$$

Hence, to regulate active power, the *d*-axis current can be adjusted; while the *q*-axis current can be adjusted for reactive power control. In addition, due to the relationship in (1), it can be seen that the active power related control should employ negative feedback control while the reactive power or ac voltage control should adopt positive feedback control.

Assuming that there is no converter power loss, the DC-link capacitor dynamics can be expressed as follows:

$$\frac{C_{dc}}{2}\frac{dV_{dc}^2}{dt} = P_{\mathrm{wind}} - P \tag{2}$$

where P_{wind} is the total power injection from the wind turbine to the dc-

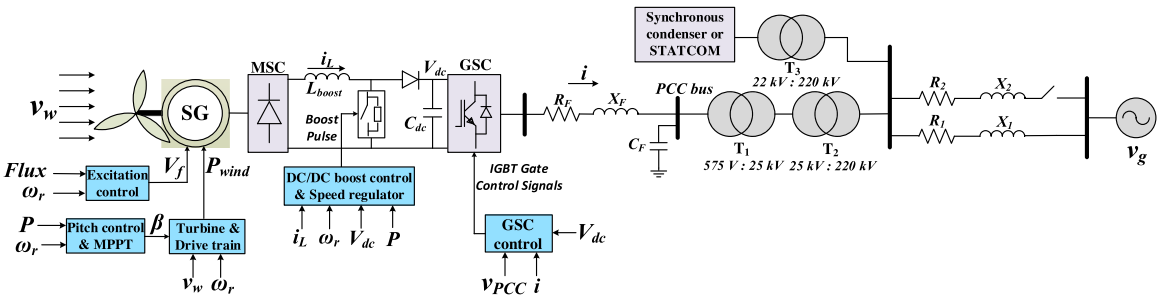

Fig. 1. EMT testbed structure of a type-4 wind farm with reactive power devices.

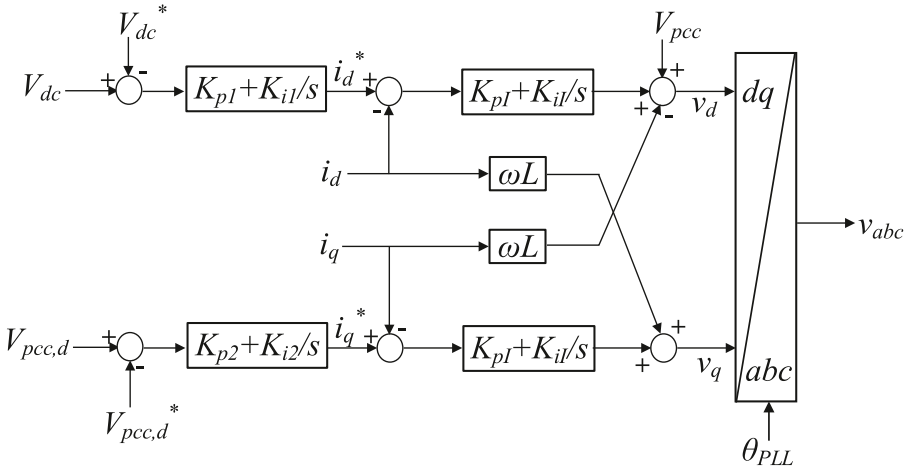

Fig. 2. GSC control structure. The dc and ac voltage references are set at 1 pu.

link capacitor and the GSC.

Equation (2) illustrates the *d*-axis current order i_d^* can be generated by DC-link voltage control. Due to the DC-link voltage relationship and the active power *P*, its can be seen that a positive feedback should be employed for DC-link voltage control. The *dq*-axis current orders (i_{dq}^*) for inner controller are from outputs of the dc and ac voltage controllers. The parameters of the wind farm and the controllers are listed in Table 1.

Table 1
Parameters of the type-4 wind farm.

Description	Parameters	Value
Rated Power	P_{Rated}	100 MW
Rated voltage	V_{Rated}	575 V
Nominal freq.	f_{nom}	60 Hz
DC-link voltage	V_{DC}	1100 V
Converter filter	L_1, R_1	0.06 mH, 0.45 mΩ
Shunt capacitor	C	90 mF
Stator winding reactance	R_s, X_{ls}	1.44 mΩ, 40.8 mΩ
Synchronous reactances	X_d, X_q	313 mΩ, 114 mΩ
Transient reactance	$X_d^{'}$	71 mΩ
Subtransient reactances	$X_d^{''}$, $X_q^{''}$	60.5 mΩ, 58.3 mΩ
Open-circuit time constant	$T_{do}^{'}$, $T_{do}^{''}$	4.49 *s*, 0.0681 *s*
Short-circuit time constant	$T_q^{''}$	0.0513 *s*
Inertia constant, poles	H, p	0.62, 2
Friction factors	F	0.01
Current PI controller	k_{pi}, k_{ii}	0.4, 48
DC voltage PI controller	$k_{p,dc}$, $k_{i,dc}$	1, 100
AC votlage PI controller	$k_{p,ac}$, $k_{i,ac}$	0.25, 25
PLL	$k_{p,PLL}$, $k_{i,PLL}$	60, 4480

2.2. STATCOM

STATCOM is widely adopted in power systems to maintain voltage profile and enhance voltage stability by offering additional reactive power. STATCOM consists of a DC capacitor and a voltage source converter, which is connected to a grid through a transformer, as shown in Fig. 3(a).

The transferred active power (*P*) and reactive power (*Q*) from the grid to the STATCOM are controlled by adjusting the output voltage of the converter. *P* and *Q* can be represented as:

$$Q = \frac{V_g\left(V_g - V_s\cos\alpha\right)}{X_s} \tag{3}$$

$$P = V_g V_s \frac{\sin(-\alpha)}{X_s} \tag{4}$$

where V_g is grid voltage amplitude at 1 p.u. and the phase angle is 0^o, V_s and α are the amplitude and phase angle of STATCOM's terminal voltage.

According to (3) and (4), it can be concluded that the amount of transferred *Q* is controlled by adjusting the magnitude of the STATCOM terminal voltage and *P* is controlled by adjusting the phase angle. Since the STATCOM is used to offer reactive power, the phase angle between sending and receiving end is zero at steady state. Hence, when the STATCOM voltage is lower than grid side, the grid sends reactive power to the STATCOM. Otherwise, the STATCOM sends reactive power to the grid.

The STATCOM tested in this paper uses a voltage source converter built of four 12-pulse three-level GTO inverters. Its detailed model is available in the demo of MATLAB/SimScape [21]. This model is developed by P. Giroux and G. Sybille of Hydro-Quebec. Fig. 4(f) shows the multi-stepped output line-to-line voltage of the 48-pulse GTO

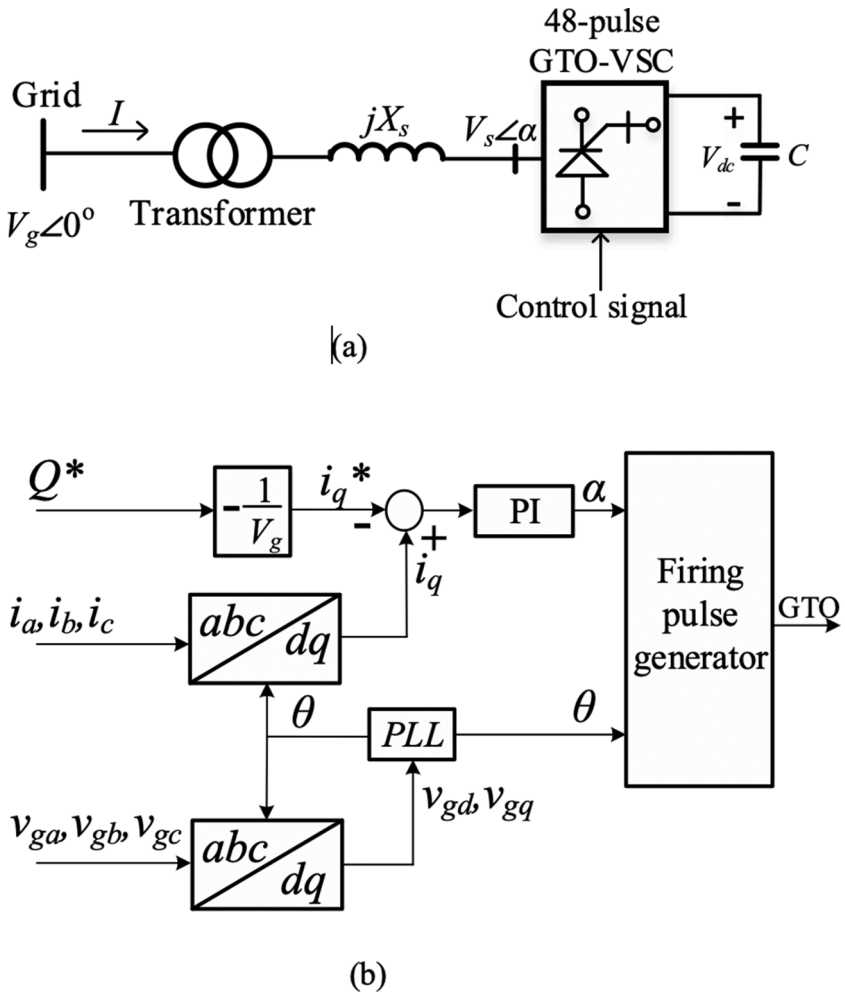

Fig. 3. (a) Single-line diagram circuit of STATCOM. (b) Reactive power control block diagram of STATCOM.

STATCOM. The zigzag phase-shifting transformers are connected to the VSC terminals. A simplified block diagram of the reactive power control is shown in Fig. 3(b) [22]. The instantaneous three-phase terminal voltage is used to generate the reference angle θ through a PLL. Line current i is decomposed into real and reactive current, and the reactive current i_q is compared with the reference reactive current i_q^* to produce an angle α, which defines the phase angle difference between converter output voltage and grid side voltage. Since the PLL aligns the grid voltage to d-axis, v_q is kept as 0, then $Q = -i_q V_g$. The reference reactive current can be generated from reference reactive power Q^*.

The magnitude and phase angle of the converter voltage determine the real and reactive power transferred between grid and STATCOM. If the STATCOM is only used for reactive power compensation, then the phase angle α is kept close to 0 (a small degree is for active power flow to compensate transformer loss), and reactive power is controlled by the voltage magnitude, which is directly proportional to capacitor voltage V_{dc}.

If the STATCOM aims to increase its reactive power to the grid, or the grid aims to decrease its reactive power to the STATCOM, V_{dc} should increase and the phase angle α should reduce to allow real power flowing from the grid to the STATCOM to charge the DC-link capacitor. The control logic in Fig. 3(b) shows that increasing Q^* causes a reduced i_q^* and α will be subject to reduction initially.

Figure 4 presents the dynamic performance of the STATCOM during operation. At $t = 2$ s, the STATCOM increases its reactive power supply to the grid from 0 pu to 0.4 pu. This change causes the angle of STATCOM voltage α to have a drop so that real power can be injected to the STATCOM to increase the capacitor voltage V_{dc}. The increased V_{dc} leads to a higher STATCOM output voltage V_s to realize reactive power generation. At $t = 4$ s, the STATCOM reverses its reactive power command to absorbs 0.4 pu reactive power from grid. In turn, its dc-link voltage and ac voltage reduce. The phase angle α is subject to change during transients but remains at around 0 at steady state.

Besides the reactive power control mode, STATCOM can also use terminal voltage control mode, as shown in Fig. 5.

The grid-side three-phase voltage v_{ga}, v_{gb} and v_{gc} are converted into dq-frame, and its magnitude is calculated as:

$$V_g = \sqrt{V_{gd}^2 + V_{gq}^2}. \tag{5}$$

The error between the reference and the measurement, $e = V_g^* - V_g$, passes to a PI controller. This PI controller generates the q-axis current order i_q^*. The inner current control employing PI control structure enforces i_q to track its order.

The parameters of the STATCOM and its controller are listed in Table 2.

2.3. SynCon

Compared to a STATCOM, a SynCon is a traditional device for reactive power generation and absorption through electromagnetic field instead of power electronics converters. For a system with limited short-circuit power capacity, SynCons are usually installed near the generation units to absorb or generate reactive power and maintain a stable

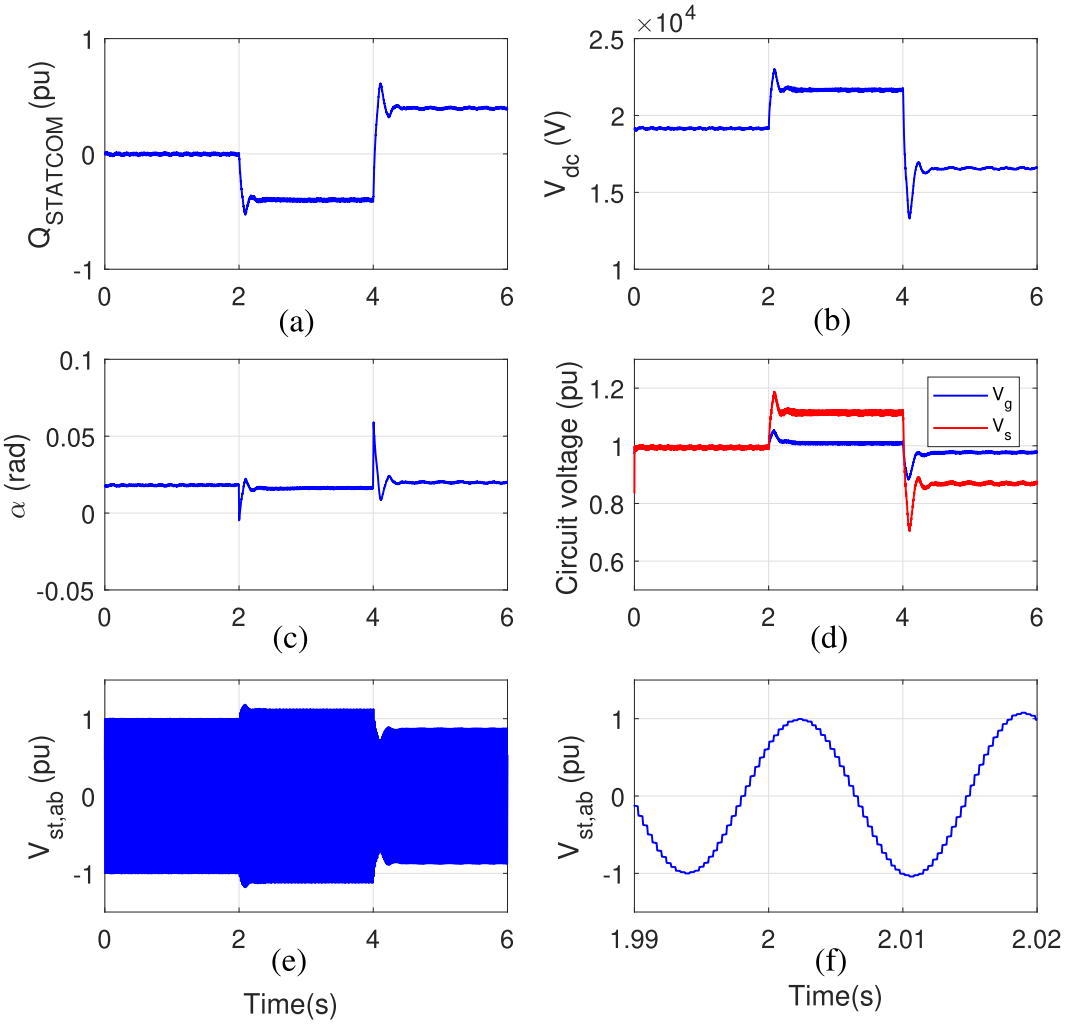

Fig. 4. (a) Reactive power from the grid to the STATCOM. (b) STATCOM capacitor voltage. (c) STATCOM terminal voltage angle. (d) Terminal voltages of STATCOM and grid. (e) STATCOM line-to-line voltage. (f) Zoom-in STATCOM line-to-line voltage.

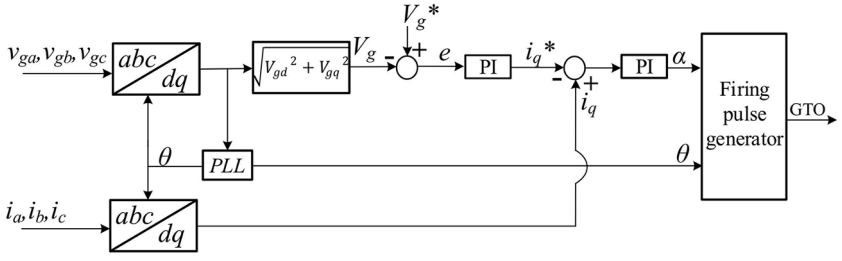

Fig. 5. Voltage control block diagram of STATCOM.

network voltage through excitation control.

A SynCon essentially is a synchronous machine working under no-load in the motor operation mode. An excitation system is used to provide excitation current and regulate the terminal voltage for the machine. According to IEEE standard, there are three different groups of excitation systems: DC type, AC type, and Static Excitation System (type ST).

In this model, the SynCon is equipped with a DC2A excitation system as shown in Fig. 6 [23]. At steady-state, both power system stabilizer voltage V_S and feedback signal V_F are zero, which means only motor terminal voltage V_C is controlled. T_B and T_C are the time constants. The parameters are listed in Table 3.

2.4. EMT simulation results

2.4.1. Wind farm only

For the 100-MW wind farm grid integration system without any reactive power devices, a dynamic event is created by tripping of a transmission line through a breaker switching. With a closed breaker, the impedance of the grid is denoted as:

$$Z_g = (R_1 + jX_1) \| (R_2 + jX_2) \tag{6}$$

If the breaker is switched off, the line impedance will be increased as:

$$Z_g = R_1 + jX_1 \tag{7}$$

Table 2
Parameters of STATCOM.

Parameters	Value (SI)
Rated Power	100 MW
Rated voltage	22 kV
Nominal freq.	60 Hz
DC capacitor	2000 μF
i_q PI controller	$5+\frac{40}{s}$
V PI controller	Para I: $12+\frac{250}{s}$
	Para II: $12+\frac{100}{s}$
PLL	$60+\frac{1400}{s}$

The grid becomes weaker through the breaker's action.

The wind farm simulation results of the PCC voltage are presented in Fig. 7. It can be observed that the system becomes unstable when X_g increases from 0.2 pu to 0.42 pu, while it keeps stable when X_g increases to 0.41 pu. Furthermore, the oscillation frequency of the unstable condition is about 9 Hz.

2.4.2. Wind farm with STATCOM

To check the effect of STATCOM, the STATCOM operating in reactive power control mode is connected to the 22-kV bus. Two cases are simulated. In the first case, there is no active and reactive power transferred between the STATCOM and the power system. Figure 8 presents the waveform of the PCC voltage and STATCOM reactive power. It can be noted that the system collapses when X_g changes from 0.2 pu to 0.42 pu due to line tripping. As illustrated in the sole wind farm case study, the wind farm marginal stability condition is at $X_g = 0.41$ pu, which means the STATCOM cannot improve the system stability performance when there is no reactive power compensation under this control strategy and this set of control parameters.

As a comparison, another case is conducted when the STATCOM injects reactive power into the system. Figure 8(b) shows that the oscillations are suppressed if the STATCOM injects 0.1 pu reactive power into the system.

Different PI controller parameters are also examined in this control system. The dynamic performance comparison is shown in Fig. 9(a). At 1 s, the X_g increases to 0.42 pu, the larger PI parameters lead to a better stability performance, and the smaller parameters may worsen the oscillation. Figure 9(b) demonstrates the larger PI parameters could increase the marginal stability condition to 0.46 pu.

In addition, two additional control modes, fixed firing angle control mode and ac voltage control mode, are examined for their impact on STATCOM's stability improvement capability.

When the system is working with fixed firing angle control as shown in Fig. 10, the control signal α is set as a constant to ensure reactive power from STATCOM at zero during operation.

Figure 11 (a) shows the system becomes stable when X_g increases to 0.42 pu with the fixed firing angle control. Figure 11(b) shows the fixed firing angle control is able to increase the marginal X_g to 0.48 pu. When X_g changes 0.49 pu, the system becomes unstable and oscillation frequency is about 17 Hz.

When the STATCOM is operating at ac voltage control mode, its voltage reference is tuned to maintain the reactive power from the STATCOM zero. Two sets of voltage controller parameters are implemented. Figure 12(a) shows the simulation results when X_g increases to 0.41 pu and 0.42 pu with Para I. It can be seen that the system stability performance is the same as that with reactive power control. But if the parameters change to Para II, the system will be stable when X_g changes to 0.42 pu as shown in Fig. 12(b). Figure 13 illustrates the system with Para II could increase the marginal stability condition to 0.49 pu. The oscillation frequency when X_g changes to 0.50 pu is about 18 Hz.

Remarks: Through simulation studies of STATCOM in different control modes and different parameters, it can be seen STATCOM can improve the stability limit of X_g from 0.42 pu to 0.49 pu, if proper control is selected. In some other cases, STATCOM may show zero improvement on stability.

2.4.3. Wind farm with SynCon

Finally, the SynCon replaces the STATCOM and operates in parallel with the wind farm. Its generated power and reactive power are regulated by an excitation system.

Figure 14 (a) shows the PCC bus voltage and reactive power from the SynCon when X_g changes from 0.2 pu to 0.42 pu. After a short period of oscillations, the system recovers to stability. To find out the marginal stability condition, the transmission line impedance is adjusted.

Table 3
Parameters of synchronous condenser.

Parameters	Value (SI)
Rated Power	20 MW
Rated voltage	22 kV
Nominal freq.	60 Hz
X_d, X_d', X_d''	654.4 mΩ, 99 mΩ, 79 mΩ
X_q, X_q''	629.6 mΩ, 79.2 mΩ
R_s, X_{ls}	1.8 mΩ, 55.4 mΩ
T_{do}', T_{do}''	4.5 s, 0.04 s
T_q', T_q''	0.67 s, 0.09 s
Inertia constant, pols	0.6, 2
Friction factors	0.6
DC capacitor	2000 μF
T_C, T_B	1, 1
K_A	300
T_E, K_E	0.01, 2
K_F	0.01

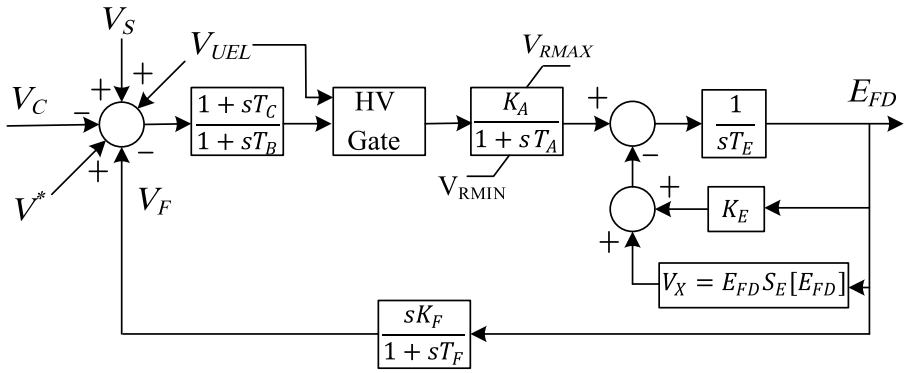

Fig. 6. Synchronous condenser exciter model.

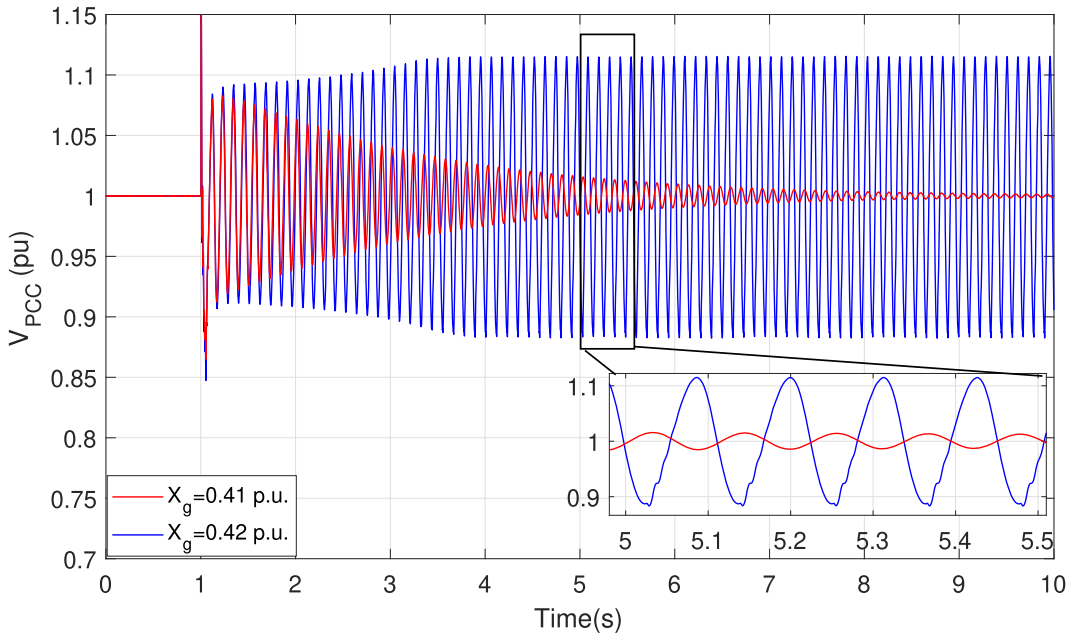

Fig. 7. Voltage at PCC bus in wind farm system. The line impedance changes at 1 s.

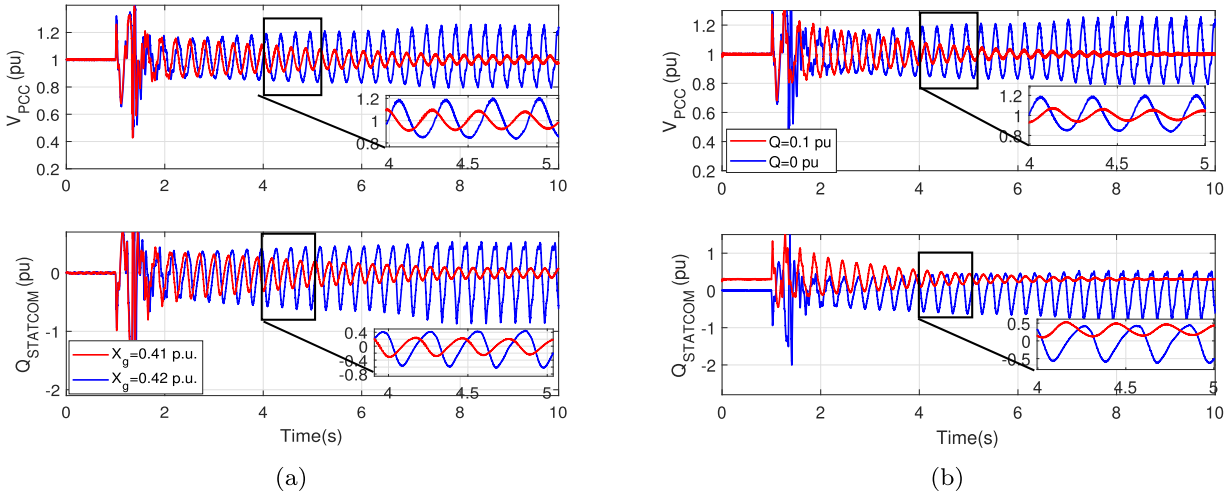

Fig. 8. STATCOM in reactive power control mode. (a) Voltage at PCC bus and reactive power from STATCOM. (b) Voltage at PCC bus in wind farm system with STATCOM when X_g changes to 0.42 pu at 1 s, STATCOM injects 0 or 0.1 pu reactive power to system.

Figure 14(b) shows the reactive power when X_g increases to 0.66 and 0.67 pu, which demonstrates that the marginal stability condition is $X_g = 0.66$ pu. The cases illustrate that the SynCon can improve the stability performance significantly even without reactive power compensation.

Remarks: Although both STATCOM and SynCon have the capability providing reactive power and improving stability performance , SynCon has advantages over STATCOM at zero reactive power condiction.

3. Admittance-based analysis

To understand the difference between SynCon and STATCOM in weak grid stability improvement, we examine their admittance models.

3.1. Admittance model extraction

The frequency scanning technique is employed to measure the admittance frequency-domain responses. The currents and voltages in the *dq*-domain are recorded after a small-signal perturbation is injected at the terminal. The obtained data are used to calculate admittance model.

As Fig. 15 shows, the controllable voltage source is connected to the wind farm at the interconnection point of 220 kV. Two perturbation voltages are superimposed into the voltage source, respectively. The voltages are defined in the *dq*-frame and converted to the *abc*-frame to form a three-phase voltage source. The resulting currents are recorded . They are converted to the *dq*-frame variables i_{dq}. Fast Fourier transform (FFT) is implemented to extract the phasor form of v_{dq} and i_{dq} at the frequency of the injected perturbation. It should be noted that the injected perturbation needs to be small enough so it has no influence on the system operation.

The admittance at every frequency point is calculated as:

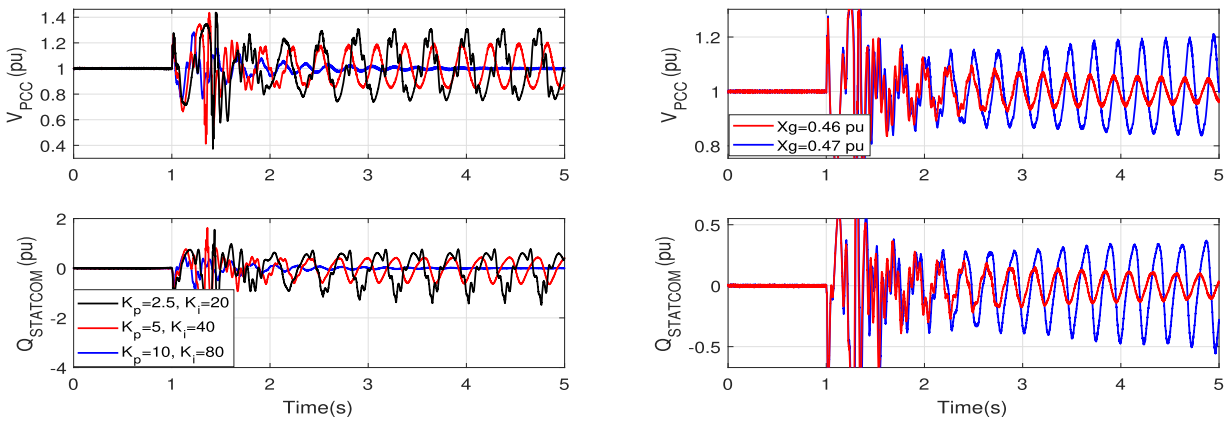

Fig. 9. (a) Comparison of different PI controllers at reactive power control mode when X_g increases to 0.42 pu. (b) X_g increases to 0.46 pu and 0.47 pu with the PI controller parameters as $k_p = 10$, $k_i = 80$.

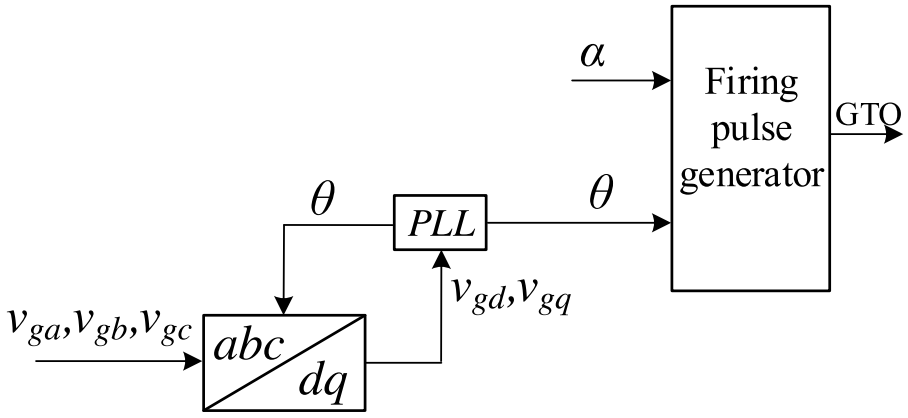

Fig. 10. STATCOM fixed firing angle control.

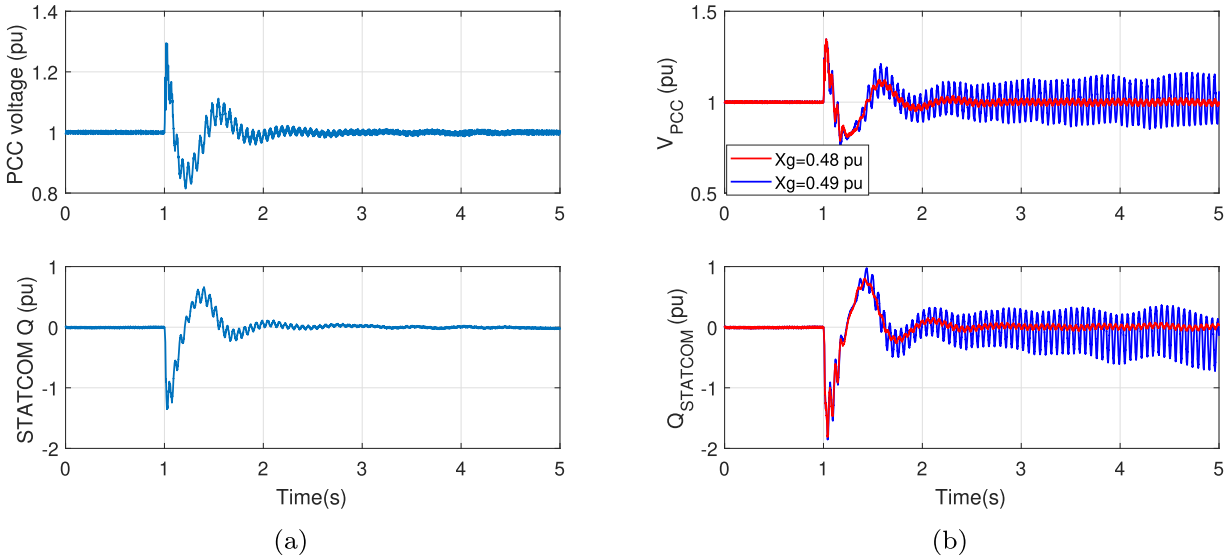

Fig. 11. STATCOM with fixed firing angle control. Voltage at PCC bus and the reactive power from the STATCOM when (a) X_g increases to 0.42 pu. (b) X_g increases to 0.48 pu and 0.49 pu.

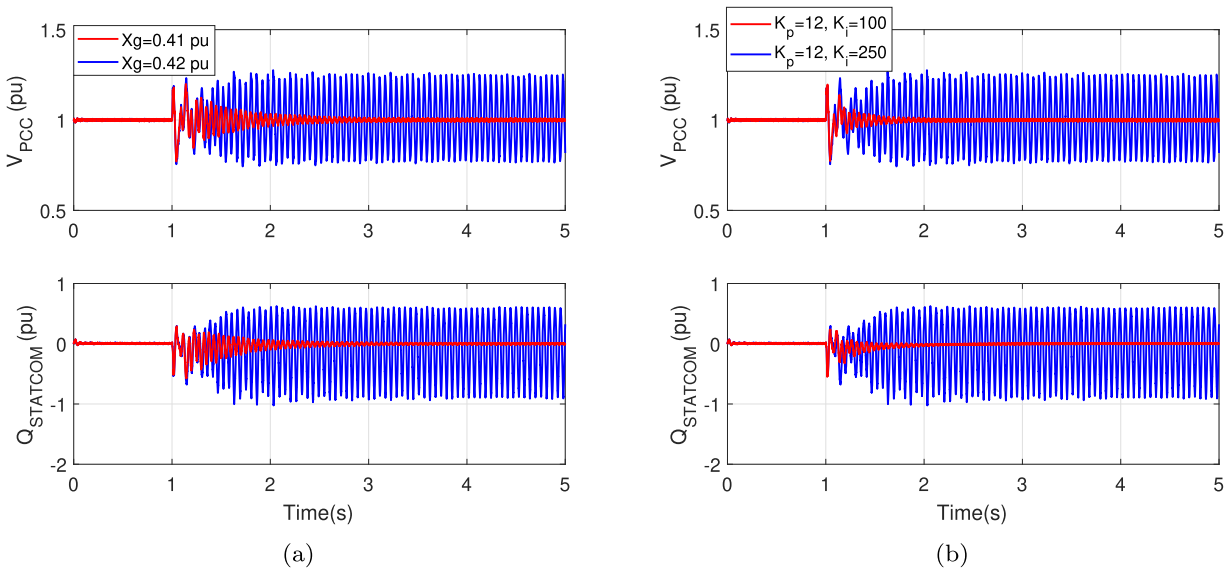

Fig. 12. STATCOM in ac voltage control mode. Voltage at PCC bus and the reactive power from the STATCOM when (a) X_g increases to 0.41 pu and 0.42 pu with Para I. (b) X_g increases to 0.42 pu with Para I and Para II.

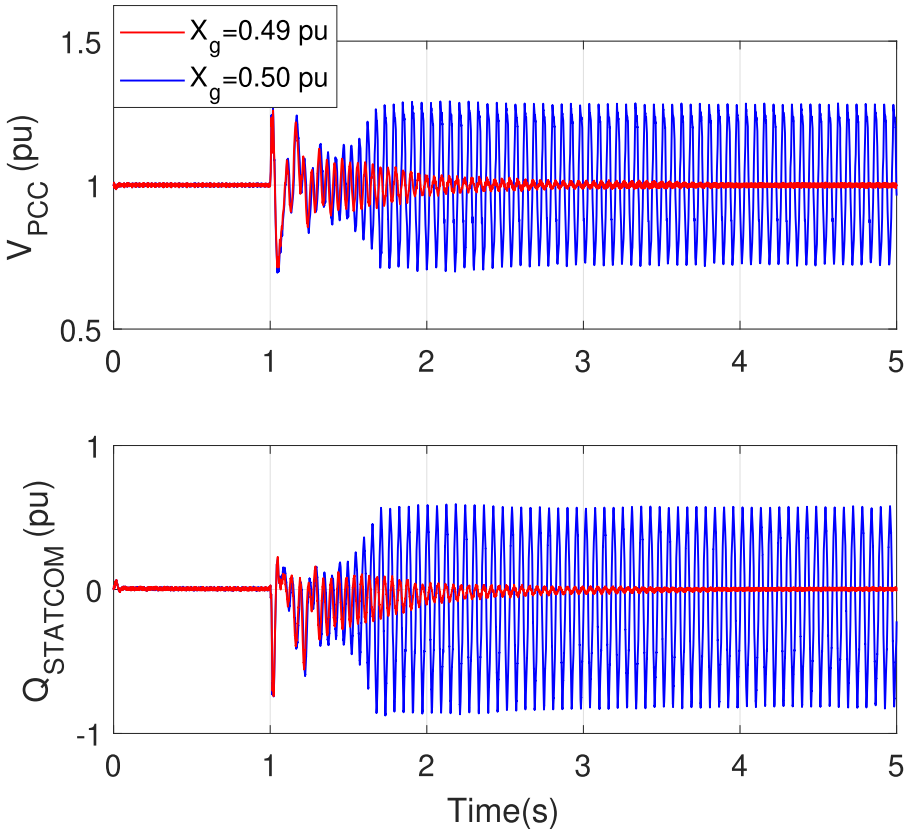

Fig. 13. STATCOM in ac voltage control model. Voltage at PCC bus and the reactive power from the STATCOM when X_g increases to 0.49 pu and 0.50 pu with Para II.

$$\begin{aligned} Y_{dd}(f_i) &= \frac{i_d^{(1)}(f_i)}{v_d^{(1)}(f_i)} \quad Y_{dq}(f_i) = \frac{i_d^{(2)}(f_i)}{v_q^{(2)}(f_i)} \\ Y_{qd}(f_i) &= \frac{i_q^{(1)}(f_i)}{v_d^{(1)}(f_i)} \quad Y_{qq}(f_i) = \frac{i_q^{(2)}(f_i)}{v_q^{(2)}(f_i)} \end{aligned} \tag{8}$$

where superscripts (1) and (2) are related to voltage perturbation in $d-$ and $q-$ axes, respectively; f_i is the injected frequency.

The injection frequencies are swept from 1 to 100 Hz with 1 Hz interval. Dq-frame voltages and currents are recorded and processed. FFT window is long enough to reduce the impact of spectral analysis. Figure 16 shows the wind farm admittance model. Each red plus sign means an injected voltage point.

The measurements can be fitted to an s-domain transfer function

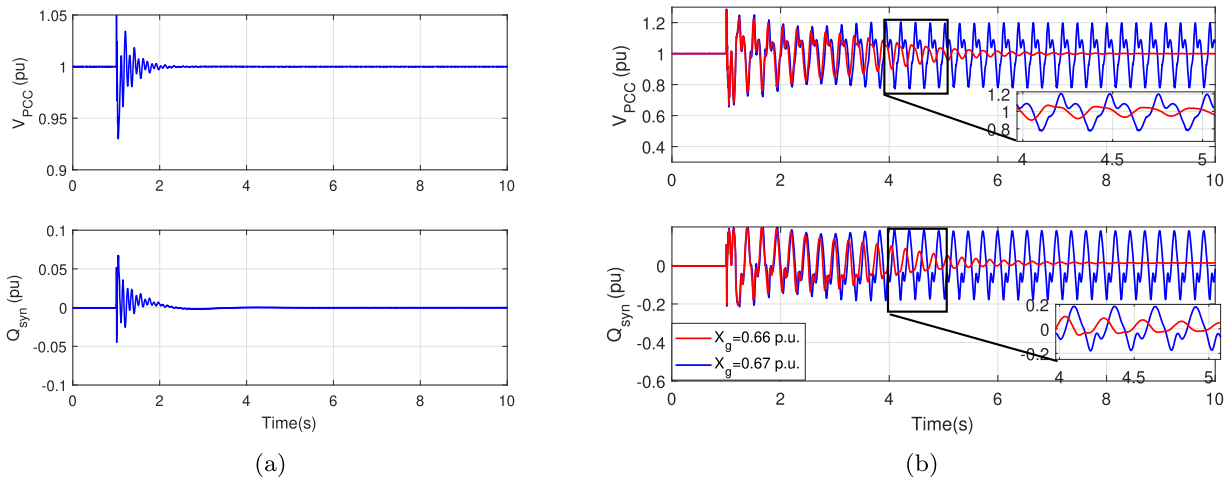

Fig. 14. (a) Voltage at PCC bus and SynCon reactive power when X_g changes from 0.20 to 0.42 pu. (b) Voltage at PCC bus and the reactive power from the SynCon for two additional cases: X_g changes from 0.20 pu to 0.66 pu and 0.67 pu, respectively.

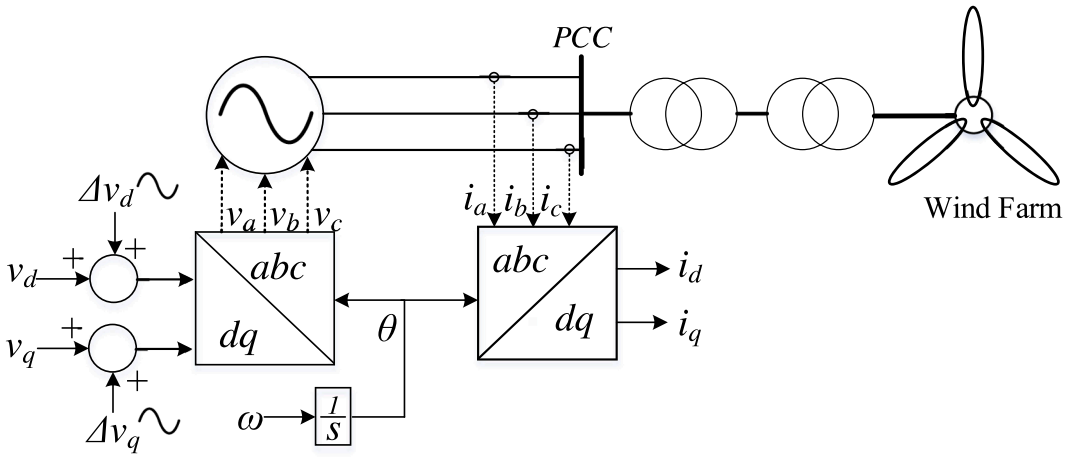

Fig. 15. *Dq*-frame admittance measurement testbed.

matrix via the vector fitting toolbox [13]. The order of the estimated system is firstly to set as 13 for each admittance of Y_{dd}, Y_{dq}, Y_{qd} and Y_{qq}. Figure 16 illustrates the comparison of the Bode plot from estimated model (blue line) and measurement data (red crosses) from harmonic injection. The estimation matches the measurements very well.

3.2. Stability analysis

This section presents *s*-domain admittance based eigenvalue analysis. The wind farm is represented by a Norton equivalent circuit consisting of a current source i_{wind} connected with an admittance Y_{wind} in parallel. The grid side is also converted to a Norton equivalent circuit with a current source i_{grid} and line admittance Y_{grid}. Thus, from the view of the PCC bus, there are two parallel-connected shunt admittance. At steady state, the system operation condition point is transferred to tge *dq*-frame by using Park transformation. The PCC voltage and the injected current in the *dq*-frame are related as:

$$\begin{bmatrix} i_d \\ i_q \end{bmatrix} = \underbrace{\left(Y_{\text{wind}} + Y_{\text{grid}}\right)}_{Y} \begin{bmatrix} v_d \\ v_q \end{bmatrix} \tag{9}$$

where

$$Y_{\text{wind}} = \begin{bmatrix} Y_{dd} & Y_{dq} \\ Y_{qd} & Y_{qq} \end{bmatrix}, \quad Y_{\text{grid}} = \begin{bmatrix} R_g + sL_g & -\omega_o L_g \\ \omega_o L_g & R_g + sL_g \end{bmatrix}$$

where ω_o is the nominal frequency.

If the system is regarded as an input/output system, where the injected current and the PCC voltage are denoted as the input and the output, respectively, then the transfer function $G(s)$ for the multi-input multi-output (MIMO) system is $Y(s)^{-1}$. The closed-loop system eigenvalues, or the poles of $G(s)$, are the roots of $\det(Y(s))$ according to Semlyen [11]. With the admittance of the wind farm being identified from measurements, the eigenvalues of the entire system can be found if the transmission line parameters are known.

Furthermore, when a reactive power device is employed in the system, then the overall admittance is:

$$Y = Y_{\text{wind}} + Y_{\text{grid}} + Y_{\text{shunt}} \tag{10}$$

where Y_{shunt} is the admittance model of the SynCon or STATCOM.

The *s*-domain model from vector fitting can used for eigenvalue analysis.

3.2.1. Wind farm only

According to (10), the eigenvalue loci are plotted in Fig. 17a with known Y_{wind}, and Y_{grid} has an increment of 0.01 pu from 0.3 pu to 0.5 pu.

It can be observed that there is one pair of complex conjugate eigenvalues affected by the varying impedance. When X_g is 0.42 pu, the oscillation mode at 9 Hz moves to right half plane (RHP), which corroborates the simulation results shown in Fig. 7.

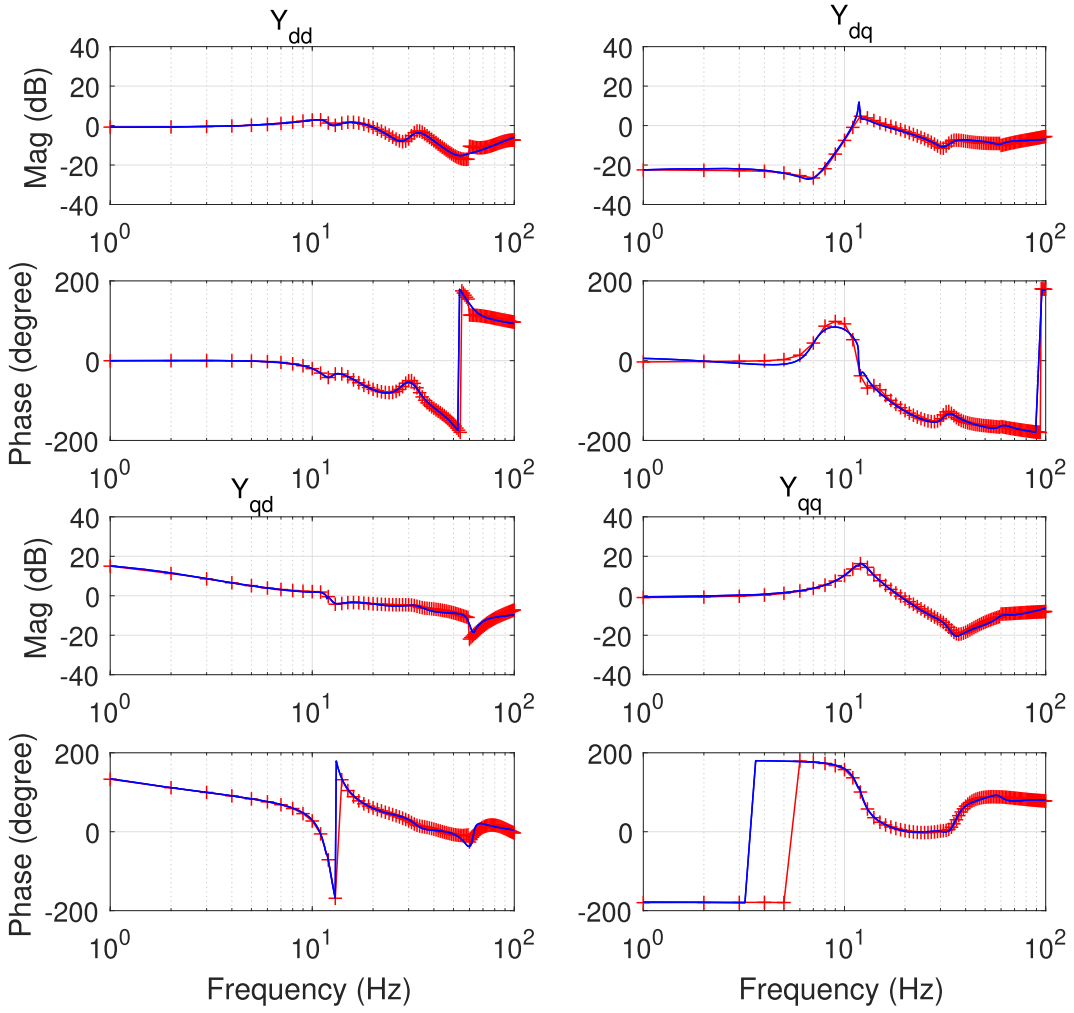

Fig. 16. Comparison of the wind farm admittance model from vector fitting and harmonic injection measurement points.

3.2.2. *Wind farm with STATCOM*

The STATCOM model is identified using harmonic injection method when it is operated in reactive power control with parameters listed in Table 2. The frequency is swept from 1 to 200 Hz with an interval of 1 Hz. Afterwards, the *dq*-admittance measurements of 200 points are obtained and processed by vector-fitting algorithm to arrive at the linear model Y_{STATCOM} in $s-$ domain.

Figure 17 (b) shows the movements of the dominant zeros of $Y_{\text{STATCOM}} + Y_{\text{wind}} + Y_{\text{grid}}$, as X_g varying from 0.3 pu to 0.5 pu. It is evident that one pair of eigenvalues crosses the imaginary axis when X_g increases to 0.42 pu, which corroborates the EMT simulation results of Fig. 8.

3.2.3. *Wind farm with SynCon*

Similar to the STATCOM, the SynCon is also measured for its admittance mdoel Y_{syn} in range of 1 to 200 Hz. Figure 17(c) shows the Eigen Loci of the overall system when X_g is changed from 0.6 to 0.8 pu. It can be observed that a pair of eigenvalues move to the RHP when X_g reaches 0.67 pu. This analytical analysis corroborates the EMT simulation results.

3.3. *Comparison of admittance of STATCOM and SynCon*

Figure 18 presents the *dq*-domain admittance models of the SynCon and STATCOM. It should be mentioned that both models have the same operating condition.

To have a better understanding, we resort to a different domain: sequence domain. The admittance model can be expressed in different domains, e.g., sequence domain or *dq*-frame. The two types of models are related [24]:

$$\begin{bmatrix} Y_{pp} & Y_{pn} \\ Y_{np} & Y_{nn} \end{bmatrix} = \frac{1}{2}\begin{bmatrix} 1 & j \\ 1 & -j \end{bmatrix}\begin{bmatrix} Y_{dd} & Y_{dq} \\ Y_{qd} & Y_{qq} \end{bmatrix}\begin{bmatrix} 1 & 1 \\ -j & j \end{bmatrix} \tag{11}$$

The sequence-domain admittance associates the two current phasors with the two voltage phasors. The two voltage (current) phasors are referred to the phasors at positive-sequence at frequency $\omega_p + \omega_1$ and negative-sequence at frequency $\omega_p - \omega_1$, where ω_1 is the nominal frequency of 60 Hz.

$$\begin{bmatrix} \bar{I}_p\left(j(\omega_p+\omega_1)\right) \\ \bar{I}_n\left(j(\omega_p-\omega_1)\right) \end{bmatrix} = \begin{bmatrix} Y_{pp}(j\omega_p) & Y_{pn}(j\omega_p) \\ Y_{np}(j\omega_p) & Y_{nn}(j\omega_p) \end{bmatrix}\begin{bmatrix} \bar{V}_p\left(j(\omega_p+\omega_1)\right) \\ \bar{V}_n\left(j(\omega_p-\omega_1)\right) \end{bmatrix} \tag{12}$$

Combining Eqs. (11) and (12), the sequence-domain current is related to the voltage through the *dq*-admittance as follow.

$$\begin{bmatrix} \bar{I}_p \\ \bar{I}_n \end{bmatrix} = \frac{1}{2}\begin{bmatrix} 1 & j \\ 1 & -j \end{bmatrix}\begin{bmatrix} Y_{dd} & Y_{dq} \\ Y_{qd} & Y_{qq} \end{bmatrix}\begin{bmatrix} 1 & 1 \\ -j & j \end{bmatrix}\begin{bmatrix} \bar{V}_p \\ \bar{V}_n \end{bmatrix} \tag{13}$$

At steady state, the operation condition is at 60 Hz. Hence, the *dq*-domain admittance at 0 Hz will be analyzed. From the Bode plot, it can be observed that the steady-state admittance is at the leftmost frequency range.

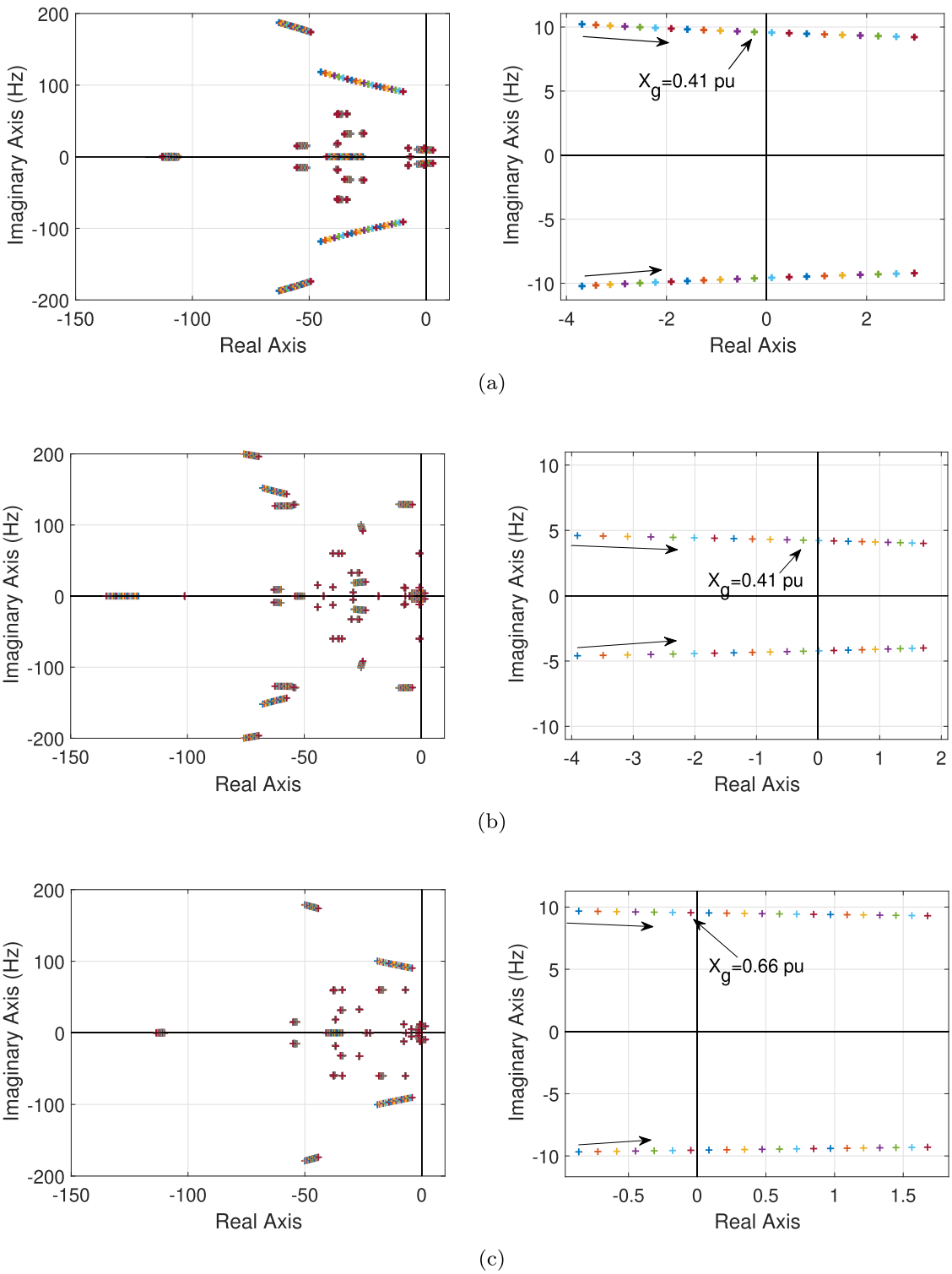

Fig. 17. Eigen loci for varying line impedance X_g for (a) wind farm, (b) wind farm with STATCOM, and (c) wind farm with SynCon. The right plots are the zoom-in of the left plots focusing on the critical mode.

The Bode plot indicates that the magnitude of Y_{dd}, Y_{dq} and Y_{qq} in SynCon are relatively small compared to Y_{qd} at steady state, thus they can be approximated to zero. The magnitude of Y_{qd} is found as -6 dB or 0.5 pu. Similarly, the magnitude of Y_{dd}, Y_{dq} and Y_{qd} in STATCOM are treated as zero and Y_{qq} is -10 dB or 0.3 pu. We may assume that the dq-domain admittance models at steady-state as follows.

$$\mathbf{Y}_{\mathbf{syn,dq}} = \begin{bmatrix} 0 & 0 \\ -0.5 & 0 \end{bmatrix}, \quad \mathbf{Y}_{\mathbf{st,dq}} = \begin{bmatrix} 0 & 0 \\ 0 & -0.3 \end{bmatrix} \tag{14}$$

Assuming the system is balanced, positive and negative-sequence voltage are $1\angle 0^o$ and 0, respectively.

For SynCon, the only non-zero element is Y_{qd} at 0 Hz. Hence:

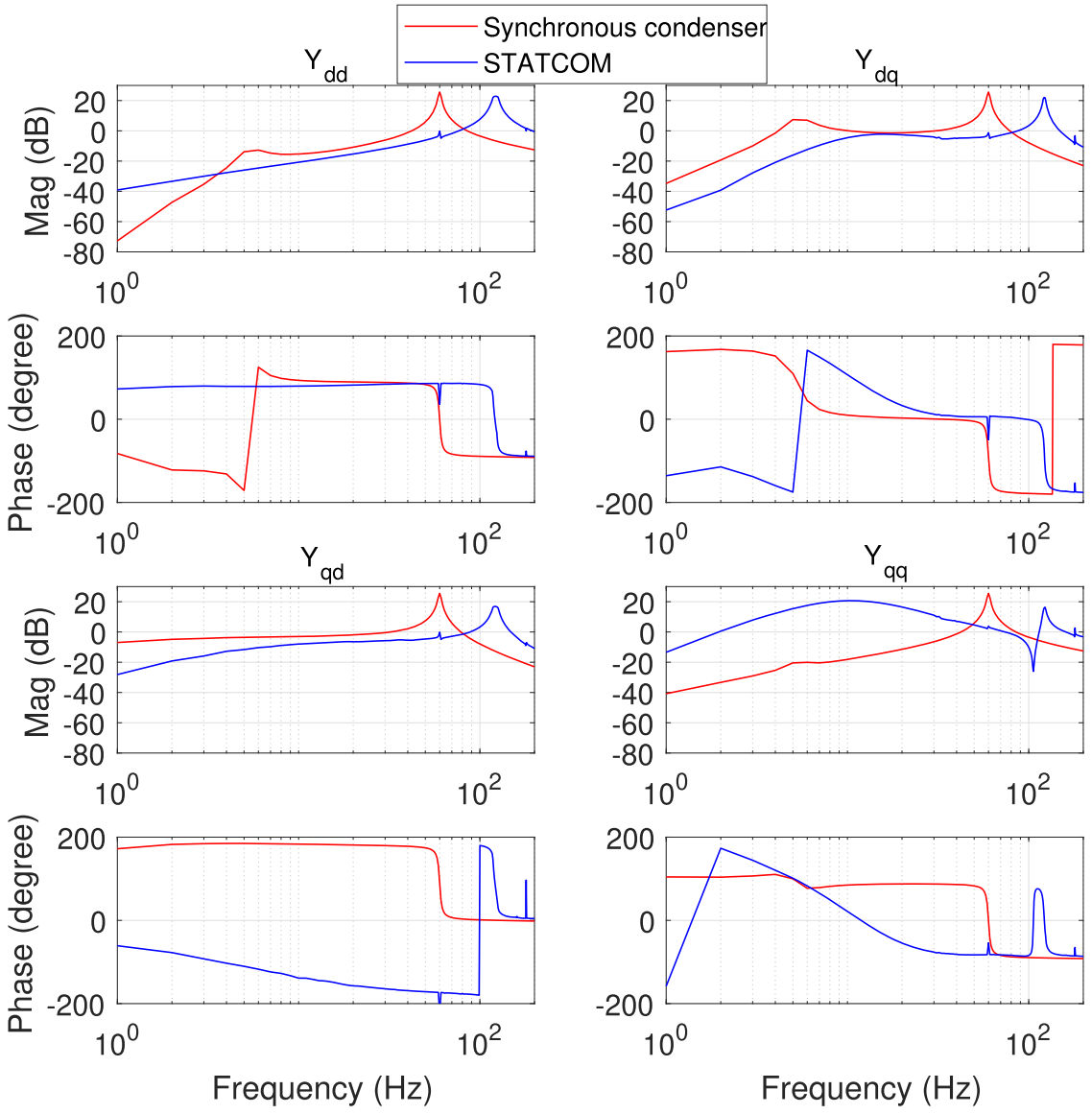

Fig. 18. *Dq*-domain admittance comparison of SynCon and STATCOM.

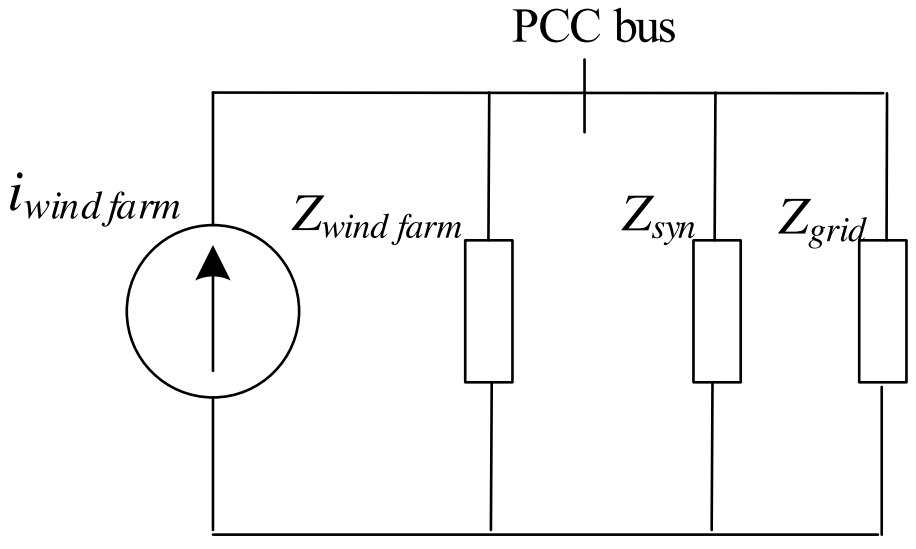

Fig. 19. Equivalent circuit model of a wind farm connected with a SynCon.

$$\begin{bmatrix} \overline{I}_p \\ \overline{I}_n \end{bmatrix} = \frac{jY_{qd}}{2} \begin{bmatrix} 1 & 1 \\ -1 & -1 \end{bmatrix} \begin{bmatrix} \overline{V}_p \\ \overline{V}_n \end{bmatrix} \tag{15}$$

$$\Rightarrow \overline{I} = \overline{I}_p + \overline{I}_n^* = jY_{qd}\overline{V}_p = -j0.5\overline{V}_p = \frac{1}{j2}\overline{V}_p \tag{16}$$

Hence, the SynCon can be regarded as an impedance connected in parallel with PCC bus. As shown in Fig. 19, by adding a parallel branch, the impedance after PCC bus will be reduced and the grid strength is improved. This is the reason why SynCon can improve stability even without injecting any reactive power.

Similarly, for the STATCOM, the sequence-domain admittance is expressed as follows.

$$\begin{bmatrix} \overline{I}_p \\ \overline{I}_n \end{bmatrix} = \frac{1}{2} \begin{bmatrix} Y_{qq} & -Y_{qq} \\ -Y_{qq} & Y_{qq} \end{bmatrix} \begin{bmatrix} \overline{V}_p \\ \overline{V}_n \end{bmatrix} \tag{17}$$

$$\Rightarrow \overline{I} = \overline{I}_p + \overline{I}_n^* = \left(\frac{1}{2}Y_{qq} - \frac{1}{2}Y_{qq}\right)\overline{V}_p = 0 \cdot \overline{V}_p \tag{18}$$

This result implies that the STATCOM does not provide an impedance in the circuit and acts as a current source at steady state or low-frequency range. Thus, the grid impedance remains the same and the stability is not improved.

Remarks: Through examining *dq*-frame admittances of a SynCon and a STATCOM, it is found that the two differ in providing (or not providing) a reactance at steady state. This difference causes the difference in stability enhancement.

4. Conclusion

As the mostly used reactive power devices, SynCon and STATCOM are implemented in a type-4 wind farm system to investigate their impacts on the overall stability of the system. Both the SynCon and the STATCOM can improve the system stability performance without reactive power compensation. On the other hand, SynCon can improve the stability margin more significantly than STATCOM. If not tuned properly, STATCOM may show zero stability improvement. This paper gives an explanation of this phenomenon based on their frequency-domain admittance models. The frequency-domain measurements are obtained from harmonic injection, and the measurement data are fitted into *s*-domain models through vector fitting method. Eigenvalue analysis results confirm the observation from the EMT simulation. It is found that SynCon and STATCOM differ in *dq*-frame admittance at low-frequency range significantly. The difference also demonstrates as SynCon providing a shunt reactance at steady state while STATCOM providing zero impedance at steady state. This equivalent impedance provided by SynCon helps increase the grid strength to allow more transferred power and enhanced stability.

CRediT authorship contribution statement

Li Bao: Software, Data curation, Writing – original draft. **Lingling Fan:** Conceptualization, Methodology, Writing – review & editing. **Zhixin Miao:** Supervision, Resources, Writing – review & editing.

Declaration of Competing Interest

We wish to confirm that there are no known conflicts of interest associated with this publication and there has been no significant financial support for this work that could have influenced its outcome.

We confirm that the manuscript has been read and approved by all named authors and that there are no other persons who satisfied the criteria for authorship but are not listed. We further confirm that the order of authors listed in the manuscript has been approved by all of us.

We confirm that we have given due consideration to the protection of intellectual property associated with this work and that there are no impediments to publication, including the timing of publication, with respect to intellectual property. In so doing we confirm that we have followed the regulations of our institutions concerning intellectual property.

We understand that the Corresponding Author is the sole contact for the Editorial process (including Editorial Manager and direct communications with the office). He/she is responsible for communicating with the other authors about progress, submissions of revisions and final approval of proofs. We confirm that we have provided a current, correct email address which is accessible by the Corresponding Author and which has been configured to accept email from linglingfan@usf.edu.

References

[1] IEEE PES WindSSO Taskforce, PES TR-80: Wind Energy Systems Subsynchronous Oscillations: Events and Modeling, 2020.
[2] L. Fan, Z. Miao, An explanation of oscillations due to wind power plants weak grid inteconnection, IEEE Trans. Sustain. Energy 9 (1) (2018) 488–490.
[3] Y. Li, L. Fan, Z. Miao, Stability control for wind in weak grids, IEEE Trans. Sustain. Energy 10 (4) (2019) 2094–2103.
[4] J. Liston, Typical synchronous condenser installations, Gen. Electr. Company Rev. 14 (1911) 234–241.
[5] 2018 state of the market report for the ERCOT electricity markets, 2019.
[6] J. Skliutas, D. LaForest, R. D'Aquila, D. Derr, E. Kronbeck, Next-generation synchronous condenser installation at the VELCO granite substation. 2009 IEEE Power Energy Society General Meeting, 2009, pp. 1–8, https://doi.org/10.1109/PES.2009.5275396.
[7] B. Singh, R. Saha, A. Chandra, K. Al-Haddad, Static synchronous compensators (STATCOM): a review, IET Power Electron. 2 (4) (2009) 297–324.
[8] G. Reed, J. Paserba, T. Croasdaile, M. Takeda, Y. Hamasaki, T. Aritsuka, N. Morishima, S. Jochi, I. Iyoda, M. Nambu, N. Toki, L. Thomas, G. Smith, D. LaForest, W. Allard, D. Haas, The VELCO STATCOM based transmission system project. 2001 IEEE Power Engineering Society Winter Meeting. Conference Proceedings (Cat. No.01CH37194) vol. 3, 2001, pp. 1109–1114vol.3, https://doi.org/10.1109/PESW.2001.917226.
[9] A. Hoke, V. Gevorgian, S. Shah, P. Koralewicz, R.W. Kenyon, B. Kroposki, Island power systems with high levels of inverter-based resources: stability and reliability challenges, IEEE Electrif. Mag. 9 (1) (2021) 74–91, https://doi.org/10.1109/MELE.2020.3047169.
[10] The age of the syncons, 2019, (https://www.energynetworks.com.au/news/energy-insider/age-syncons/), Accessed: 2021-09-02.
[11] A.I. Semlyen, s-domain methodology for assessing the small signal stability of complex systems in nonsinusoidal steady state, IEEE Trans. Power Syst. 14 (1) (1999) 132–137, https://doi.org/10.1109/59.744501.
[12] L. Fan, Z. Miao, Admittance-based stability analysis: bode plots, nyquist diagrams or eigenvalue analysis? IEEE Trans. Power Syst. 35 (4) (2020) 3312–3315, https://doi.org/10.1109/TPWRS.2020.2996014.
[13] B. Gustavsen, A. Semlyen, Rational approximation of frequency domain responses by vector fitting, IEEE Trans. Power Deliv. 14 (3) (1999) 1052–1061, https://doi.org/10.1109/61.772353.
[14] L. Ljung, R. Singh, Version 8 of the matlab system identification toolbox, IFAC Proc. Vol. 45 (16) (2012) 1826–1831.
[15] J. Dixon, L. Moran, J. Rodriguez, R. Domke, Reactive power compensation technologies: State-of-the-art review, Proc. IEEE 93 (12) (2005) 2144–2164, https://doi.org/10.1109/JPROC.2005.859937.
[16] Y. Zhang, A.M. Gole, Comparison of the transient performance of STATCOM and synchronous condenser at HVDC converter stations. 11th IET International Conference on AC and DC Power Transmission, 2015, pp. 1–8, https://doi.org/10.1049/cp.2015.0069.
[17] Y. Liu, S. Yang, S. Zhang, F.Z. Peng, Comparison of synchronous condenser and STATCOM for inertial response support. 2014 IEEE Energy Conversion Congress and Exposition (ECCE), 2014, pp. 2684–2690, https://doi.org/10.1109/ECCE.2014.6953761.
[18] C. Li, R. Burgos, B. Wen, Y. Tang, D. Boroyevich, Analysis of STATCOM small-signal impedance in the synchronous d-q frame, IEEE J. Emerg. Sel. Topi.Power Electron. 8 (2) (2020) 1894–1910, https://doi.org/10.1109/JESTPE.2019.2942332.
[19] C. Li, R. Burgos, Y. Tang, D. Boroyevich, Application of d-q frame impedance-based stability criterion in power systems with multiple STATCOMS in proximity. IECON 2017 - 43rd Annual Conference of the IEEE Industrial Electronics Society, 2017, pp. 126–131, https://doi.org/10.1109/IECON.2017.8216026.
[20] L. Bao, L. Fan, Z. Miao, Comparison of synchronous condenser and STATCOM for wind farms in weak grids. NAPS 2020, 2020.
[21] MATLAB, Statcom (detailed model), https://www.mathworks.com/help/physmod/sps/ug/statcom-detailed-model.html;jsessionid=2a1b35ac24097edc871901940247.

[22] N.G. Hingorani, L. Gyugyi, Static Shunt Compensators: SVC and STATCOM, 2000, pp. 135–207.
[23] IEEE recommended practice for excitation system models for power system stability studies, IEEE Std 421.5-1992, 1992, pp. 1–56.
[24] A. Rygg, M. Molinas, C. Zhang, X. Cai, A modified sequence-domain impedance definition and its equivalence to the dq-domain impedance definition for the stability analysis of ac power electronic systems, IEEE J. Emerg. Sel. Top.Power Electr. 4 (4) (2016) 1383–1396, https://doi.org/10.1109/JESTPE.2016.2588733.